5358 *Macromolecules* **2010**, *43*, 5358–5364
DOI: 10.1021/ma1007286

Macromolecules
ARTICLE

# Preparation and Morphology Control of Block Copolymer/Metal Salt Hybrids via Solvent-Casting by Using a Solvent with Coordination Ability

**Atsushi Noro,[†] Yoshio Sageshima,[†] Shigeo Arai,[‡] and Yushu Matsushita*,[†]**

[†]*Department of Applied Chemistry, Graduate School of Engineering and* [‡]*Ecotopia Science Institute, Nagoya University, Furo-cho, Chikusa-ku, Nagoya 464-8603, Japan*

*Received April 5, 2010; Revised Manuscript Received May 9, 2010*

ABSTRACT: We report a systematic study on preparation and morphology control of macroscopically homogeneous hybrid films composed of a block copolymer and a metal salt, where one block interacts with a metal salt by metal-to-ligand coordination. Hybrids were prepared by blending a polystyrene-*b*-poly(4-vinylpyridine) (PS−P4VP, $M_n = 37$K, $\phi_s = 0.79$) block copolymer and iron(III) chloride ($FeCl_3$) with changing the mole fraction of $FeCl_3$. To prevent the rapid cross-linking formation between P4VP and $FeCl_3$, pyridine as a polar solvent with the coordination ability was used at the solvent-casting stage, which turned out to be effective to prepare macroscopically homogeneous films with a large amount of $FeCl_3$. Transmission electron microscopy and small-angle X-ray scattering measurements were carried out to observe the morphology of thermally annealed samples at the nanoscopic scale. It was revealed that simple two-phase nanostructures were observed due to homogeneously mixing of $FeCl_3$ into a P4VP phase up to 0.9 mol equiv of $FeCl_3$ to pyridine units in P4VP. This indicates $FeCl_3$ works as a filler in a P4VP phase just as small homopolymers: domain expansion and morphology transition were observed as the amount of added $FeCl_3$ increases. However, overflow of $FeCl_3$ was observed in the hybrid with an amount of 1.0 mol equiv of $FeCl_3$. This is probably due to the saturation of incorporated $FeCl_3$, indicating that morphology of the present system can be controlled by stoichiometric balance between 4-vinylpyridine units and $FeCl_3$.

## Introduction

Organic−inorganic hybrids are the attractive materials that would have flexibility and processability of organic materials in addition to the useful features of inorganic materials.[1−3] Especially in the case of using metals as inorganic components, the prominent features of metals such as electronic,[4] magnetic,[5] and optical[6] properties could be built in those materials.[7−9] Therefore, these hybrid materials containing metals have been vigorously studied because such hybrids could become high performance and high functional materials with novel distinctions of their own. If block copolymers[10−16] are used as organic components in order to utilize the feature of nanosize regularity on hybrid preparation, these hybrids could easily provide novel properties derived from nanosize effects, especially optoelectrical and microelectrical properties.[17−24]

In fact, there are many efforts for preparing hybrids of block copolymers/metallic components to understand the relationships between the morphology and macroscopic physical properties of the hybrids.[25−30] Among them, one of the investigations is to synthesize a block copolymer bearing a block composed of a monomer sequence containing transition metals, which easily provides nanophase-separated structures with metals.[31−35] There are other types of investigations which is common to build up hybrids by blending a block copolymer and metal nanoparticles.[36−48] Russell and Emrick et al. prepared spin-coated films with nanophase-separated structures from blends of PS−P2VP block copolymers/surfactant-capped nanoparticles.[49,50] On the other hand, Kramer et al. succeeded in preparation of the hybrids consisting of block copolymers with polymer-coated nanoparticles and reported on the distribution of nanoparticles in the domain.[51−54] There are other types of studies concerning hybrids composed of block copolymers and nanoparticles by blending metal precursors.[55−62] Although the common metal salts cannot provide directly prominent features of metals as they are, they could be used to prepare block copolymer/metal hybrids. In the preparation procedure of these hybrids, special care should be taken about cross-linking of polymers induced at higher molar amounts of metal salts due to the ability of double or triple coordination to ligands in a polymer. For example, more than 0.2 mol equiv of a cadmium chloride per monomer unit resulted in occurring heterogeneous precipitation according to the previous works by Lee and Kim et al.[63,64] Therefore, it is useful if there is a universal procedure to prepare macroscopically homogeneous hybrid films with a large amount of metals by blending a block copolymer and a simple metal salt.

In this article, we propose a useful preparation procedure of block copolymer/metal salt hybrids via metal-to-ligand coordination in a polar solvent with the coordination ability, pyridine, to obtain macroscopically homogeneous hybrid films. Polystyrene-*b*-poly(4-vinylpyridine) (PS−P4VP) and iron(III) chloride ($FeCl_3$) as a readily available metal salt were blended, and the morphology of their solvent-cast films with a different amount of $FeCl_3$ was investigated by transmission electron microscopy (TEM) and small-angle X-ray scattering (SAXS).

## Experimental Section

**Materials.** 4-Vinylpyridine was purchased from Aldrich, while the other regents including iron(III) chloride were purchased from Kishida Regents Chemicals. Styrene and 4-vinylpyridine for polymerization were purified by passing through an aluminum oxide column before use. Pyridine as a casting solvent was used after removing water with molecular sieves. The others were used as received.

*Corresponding author. E-mail: yushu@apchem.nagoya-u.ac.jp.

 Published on Web 05/20/2010 

**Scheme 1. Synthesis of a PS−P4VP Block Copolymer**

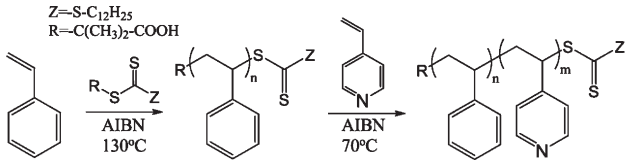


**Table 1. Codes and Characteristics of Blend Samples of PS−P4VP/$FeCl_3$**

| code | $x_{pyridine}$: $x_{FeCl_3}$ [a] | $w_{PS\text{-}P4VP}$: $w_{FeCl_3}$ [b] | $w_{PS}$:$w_{P4VP}$: $w_{FeCl_3}$ [c] | morphology[d] | $D$[e]/nm |
|---|---|---|---|---|---|
| PS−P4VP | 1:0 | 100:0 | 77.3:22.7:0 | S | 24.3 |
| Fe(0.1) | 1:0.1 | 96.6:3.4 | 73.1:23.5:3.4 | S | 22.9 |
| Fe(0.2) | 1:0.2 | 93.2:6.8 | 70.5:22.7:6.8 | S | 22.5 |
| Fe(0.3) | 1:0.3 | 90.2:9.8 | 68.2:22:9.8 | S | 24.6 |
| Fe(0.4) | 1:0.4 | 88:12 | 66:22:12 | S | 27.2 |
| Fe(0.5) | 1:0.5 | 85:15 | 64:21:15 | C | 42.4 |
| Fe(0.6) | 1:0.6 | 82:18 | 62:20:18 | C | 43.1 |
| Fe(0.7) | 1:0.7 | 80:20 | 60:20:20 | L | 41.9 |
| Fe(0.8) | 1:0.8 | 78:22 | 59:19:22 | L | 42.4 |
| Fe(0.9) | 1:0.9 | 76:24 | 57:19:24 | L | 45.5 |
| Fe(1.0) | 1:1.0 | 73:27 | 56:17:27 | M(C, L) | |

[a] Mole ratio of $FeCl_3$ to pyridine units. [b] Weight ratio of PS−P4VP:$FeCl_3$. [c] Weight ratio of PS:P4VP:$FeCl_3$, calculated from the mole fractions of PS−P4VP and a weight ratio of PS−P4VP:$FeCl_3$ in this table. [d] L: lamellar structure; C: cylindrical structure; S: spherical structure; M: macrophase separation. [e] Distance between domains for each morphology at room temperature estimated from Figure 6.

**Synthesis and Characterization of a Parent Polymer.** A polystyrene-*b*-poly(4-vinylpyridine) (PS−P4VP) block copolymer was synthesized via reversible addition−fragmentation chain transfer (RAFT) polymerization[65−68] by using the monofunctional chain transfer agent, *S*-1-dodecyl-*S*′-(α,α′-dimethyl-α″-acetic acid)trithiocarbonate (Scheme 1, see also Supporting Information).[69] Details in similar synthesis about RAFT polymerization were described in the previous literatures.[70,71] The polymer was purified by a reprecipitation procedure with hexane as a nonsolvent and dried *in vacuo*. The polydispersity indices (PDIs) of polymers were determined by using three TSKgel G4000$H_{HR}$ columns (Tosoh Corp.) combined with an HPLC pump and an UV detector using the wavelength of 220 nm. The eluent was dimethylformamide (DMF), and the flow rate was 1 mL/min. The number-average molecular weight of the polymer was determined with $^1$H NMR (Varian) by end-group analysis.[72] The volume fraction of the PS block ($\phi_s$) in the PS−P4VP block copolymer was also determined by $^1$H NMR. Molecular characteristics of PS−P4VP, i.e., $M_n$, PDI, and $\phi_s$, were determined to be 37 000, 1.17, and 0.79, respectively.

**Preparation of Hybrid Samples.** Block copolymer/metal salt hybrids were prepared by a solvent-casting method. Iron(III) chloride ($FeCl_3$) was used as a readily available metal salt. Chloroform and pyridine, both of which are good solvents for PS, P4VP, and $FeCl_3$, were used as solvents at the first trial of blend experiments to compare solvent effects. After checking solvent effects, pyridine was chosen and used for all the other blend experiments. In fact, the following procedure was used: a 4 wt % PS−P4VP solution in pyridine and a 2 wt % $FeCl_3$ solution were prepared separately, and then these were blended together in a Teflon Petri dish. The solvent was evaporated slowly on a hot plate at 50 °C for 24 h, and solvent-cast films were thermally annealed at 165 °C for 60 h *in vacuo*. To investigate the dependence on mole ratios of $FeCl_3$:pyridine in PS−P4VP, the mole ratio of $FeCl_3$ to pyridine units in PS−P4VP was varied as *X*:1 ($X$ = 0.1−1.0) in the blends, and these hybrids were coded as Fe($X$) in Table 1.

**Morphology Observation.** Thermally annealed films were cut into ultrathin sections with a thickness of ca. 50 nm by using a microtome, Reica Ultracut FCS, in a dry atmosphere. A transmission electron microscope (TEM) of H-800 (Hitachi) was used under an acceleration voltage of 100 or 150 kV to observe the morphology in ultrathin sections of the hybrid films. An energy dispersive X-ray spectrometer (EDX) installed in the TEM was also used to detect the characteristic X-rays of metal elements in hybrids generated by the electron beams. Small-angle X-ray scattering (SAXS) measurements were carried out at the beamline 15 A in the Photon Factory, Tsukuba, Japan. The wavelength of the incident X-rays was 0.150 nm, the camera length was 2.38 m, and imaging plates were used as detectors. Samples were exposed to the incident beam from the direction parallel to the film surface.

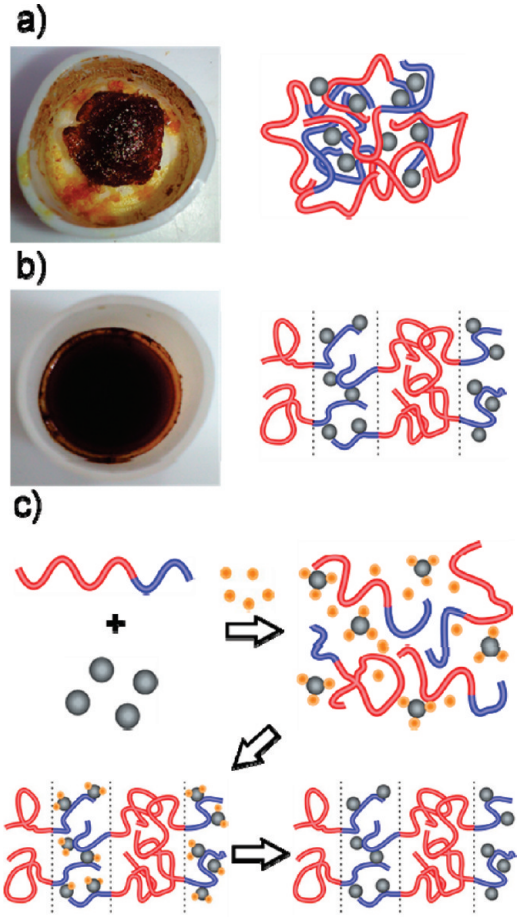


**Figure 1.** Optical images and schematic illustrations of hybrids after evaporating solvents: chloroform (a) and pyridine (b). A proposed mechanism for a solvent-casting process from pyridine solutions was also illustrated in (c). $FeCl_3$ was drawn as a silver sphere, while a pyridine molecule was also drawn as an orange sphere but with a smaller size. The second step in the scheme represents the solution in pyridine at a dilute condition, where pyridine-coordinated $FeCl_3$ and PS−P4VP dissolve homogeneously. The third step illustrates the final stage of solvent-casting, where most of free pyridine molecules and some of pyridine molecules coordinating to $FeCl_3$ at the second step have already gone and $FeCl_3$ is located on P4VP blocks because of the coordination interaction. After thermal annealing and complete removal of pyridine molecules, a simple two-phase nanostructure comprised of organic (PS) and hybrid (P4VP/$FeCl_3$) phases is attained as shown at the fourth step.

## Results

**Solvent Casting with Chloroform and Pyridine.** Figure 1 compares optical images of hybrids at the mole ratio of 0.5:1 for $FeCl_3$:pyridine units in a PS−P4VP/$FeCl_3$ complex after solvent casting. When chloroform was used as a solvent, heterogeneous aggregates or precipitates appeared in the solution just after blending the solution of PS−P4VP and that of $FeCl_3$ (Figure 1a). It is well-known that pyridine units

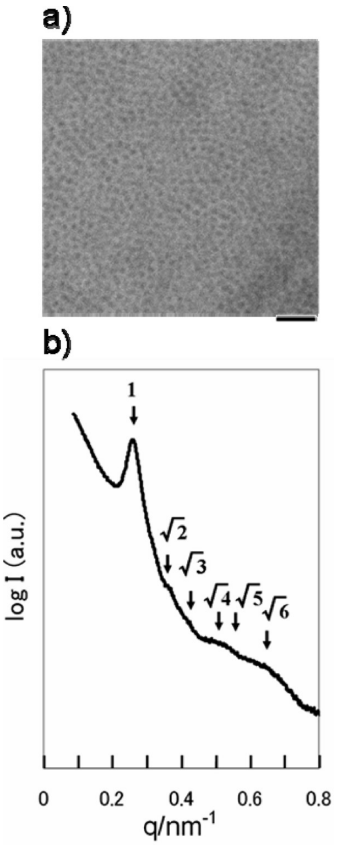


**Figure 2.** A TEM image (a) and a SAXS profile (b) of PS−P4VP. Note the sample for TEM observation was stained with an iodine vapor so that the darker phase represents P4VP. A scale bar is 100 nm.

in PS−P4VP interact strongly with metal salts such as $FeCl_3$ by metal-to-ligand coordination. In addition, metal salts are also known to induce cross-linking of polymers easily[63,64] because the coordination number of metal salts is usually larger than two or three for the case of $FeCl_3$. To avoid cross-linking of P4VP blocks, a much more polar solvent, pyridine, was used in the solvent-casting step. Pyridine actually plays a roll of an inhibitor because it forms a complex with $FeCl_3$ via coordination and hence prevents polymers from cross-linking by $FeCl_3$. No precipitates were seen in the solution during solvent-casting when pyridine was used as a solvent, and therefore a macroscopically homogeneous film was prepared after evaporating the solvent as shown in Figure 1b. The homogeneous films with a large mount of a metal salt such as 0.5 mol equiv of pyridine units in PS−P4VP had not been easily obtained so far[63,64] because cross-linking of polymers is easily induced by the addition of a metal salt, which also causes poorly ordered nanostructures.[73] A proposed solvent-casting mechanism is schematically shown in Figure 1c. Note casting speed was so slow at RT because pyridine molecules interact with $FeCl_3$, so that a higher temperature than RT, 50 °C, was used during casting to make casting speed faster. The other hybrids were also prepared by solvent-casting from pyridine solutions.

**Morphology Observation of a PS−P4VP Parent Copolymer.** Figure 2 displays a bright-field TEM image with a SAXS profile for a PS−P4VP parent copolymer. A bulk film of PS−P4VP shows a spherical nanophase-separated structure with a PS matrix (Figure 2a), where brighter and darker phases represent PS and P4VP phases, respectively, since the specimen was stained with an iodine ($I_2$) vapor. Figure 2b shows a SAXS profile of the same block copolymer. The vertical axis represents an arbitrary intensity in a logarithmic scale, and the horizontal axis is a scattering vector, $q$ ($= 4\pi \sin\theta/\lambda$), where $\lambda$ and $2\theta$ are the wavelength of X-rays and scattering angle, respectively. The profile shows peaks at the relative $q$ position of 1, $2^{1/2}$, $3^{1/2}$, $4^{1/2}$, $5^{1/2}$, and $6^{1/2}$ referring to the first-order peak at 0.25 $nm^{-1}$, indicating bcc packing of spheres. Although the intensities of some peaks such as at $2^{1/2}$ and $3^{1/2}$ are weak, this could be understood by the contributions from the particle scattering of isolated spheres and the composition ratio of spherical domains and a matrix, according to the detailed morphology study by SAXS about block copolymer/homopolymer blends.[74] This SAXS result and analysis are consistent with those of TEM in Figure 2a.

**Morphology Observation of PS−P4VP/$FeCl_3$ Hybrids (Fe($X$)).** Figure 3 compares TEM images of nine hybrids. While the thin section of a PS−P4VP parent copolymer was stained with an $I_2$ vapor to give a good contrast between different phases, these TEM images show nanophase-separated structures with sufficient electron density contrasts between brighter and darker phases, regardless of no staining at all. Therefore, the electron-rich (or darker) phase is assumed to be a P4VP phase which should contain an iron element due to preparation conditions. Morphology transition was evidently observed for these hybrids according to the weight fraction of $FeCl_3$: spherical structures with PS matrices for Fe(0.1), Fe(0.2), Fe(0.3), and Fe(0.4); cylindrical structures with PS matrices for Fe(0.5) and Fe(0.6); alternating lamellar structures for Fe(0.7), Fe(0.8), and Fe(0.9). At Fe(1.0), however, an excess amount of $FeCl_3$ was overflowed from nanophase-separated regions of the hybrid, as can be seen in Figure 4a. In addition, both cylindrical and lamellar structures were clearly recognized as shown in Figure 4b,c.

To further confirm whether the darker phase contains metal components or not, EDX was measured during TEM observation. Figure 5 shows an EDX spectrum, a bright-field image, and the corresponding elemental-mapping (Fe-mapping) image to the bright-field image for Fe(0.8). Fe(0.8) was chosen because the morphology was an simple alternating lamellar structure as shown in Figure 3h, and the sample contains a comparatively large amount of $FeCl_3$. Before obtaining a mapping image, the X-ray spectrum was measured. There are two peaks at 6.4 and 7.0 keV on the EDX spectrum in Figure 5a, indicating the existence of an iron element in the observed area. There is also a peak at 2.7 keV, indicating the coexistence of a chlorine element. For acquiring a mapping image, characteristic X-ray at 6.4 keV from an iron element was collected in the observed area of Figure 5b. The brighter phase at the Fe-mapping image in Figure 5c mostly overlaps with the darker phase at the bright-field image in Figure 5b. These results indicate that Fe-containing phase corresponds to electron-rich (or darker) phase in the bright-field image.

Figure 6 compares SAXS profiles of all Fe($X$) hybrids. The profiles in Figure 6a,b are displayed in the order of mole ratios from bottom to top: Fe(0.1), Fe(0.2), Fe(0.3), Fe(0.4), with Fe(0.5) in Figure 6a; Fe($X$) ($X = 0.6-1.0$) in Figure 6b. Profiles of Fe(0.1), Fe(0.2), Fe(0.3), and Fe(0.4) in Figure 6a have peaks at relative $q$ values of 1, $2^{1/2}$, $3^{1/2}$, $4^{1/2}$, $5^{1/2}$, and $6^{1/2}$, suggesting bcc spherical structures. The weak intensities of some peaks such as at $2^{1/2}$ and $3^{1/2}$ are attributed to the contributions from the particle scattering and the composition of spherical structures.[74] By using the equation of $d_{100} = 2\pi/q$, where $d_{100}$ is the edge distance of the bcc lattice, the intersphere domain distance, $D$ ($= (3/4)^{1/2} d_{100}$), was estimated as shown in Table 1. By comparing Figures 2b and 6a, we notice the peak positions on the profiles shift to

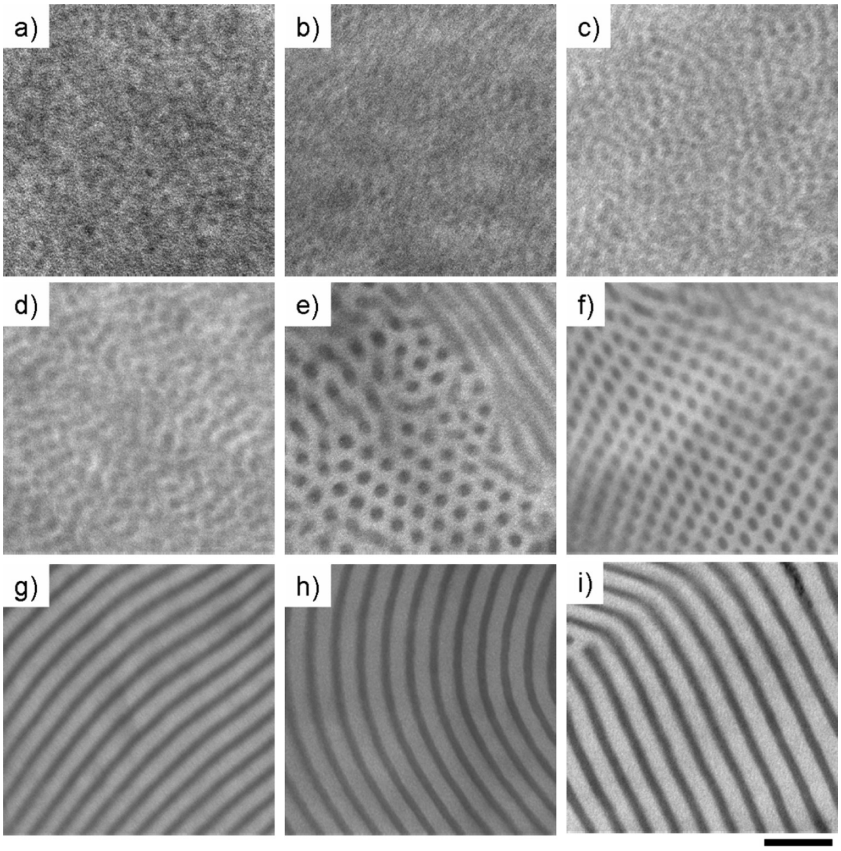


**Figure 3.** TEM images of Fe($X$) ($X$ = 0.1−0.9): (a) Fe(0.1), (b) Fe(0.2), (c) Fe(0.3), (d) Fe(0.4), (e) Fe(0.5), (f) Fe(0.6), (g) Fe(0.7), (h) Fe(0.8), and (i) Fe(0.9). A scale bar represents 100 nm. Note the samples were not stained at all with any vapors but have good contrasts of the electron density between two phases due to the incorporation of $FeCl_3$ into a darker phase.

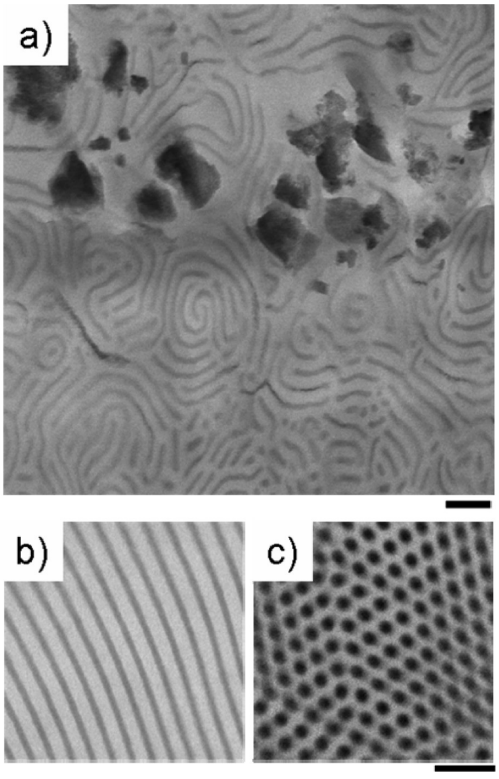


**Figure 4.** TEM images of Fe(1.0): (a) overflow of $FeCl_3$; (b) a lamellar structure in a nanophase-separated region; (c) a cylindrical structure in a nanophase-separated region. Both scale bars are 100 nm.

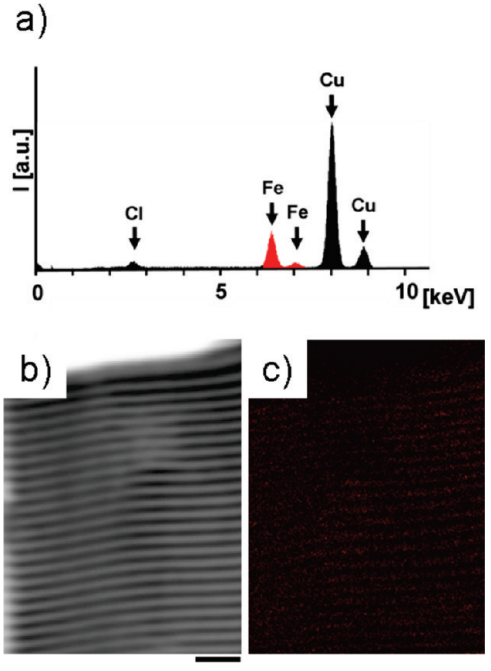


**Figure 5.** EDX spectrum of Fe(0.8) (a), a bright-field image (b), and an elemental-mapping image (c). Red dots at a brighter phase in (c) express X-rays from an iron element. A scale bar represents 100 nm. Note there is a resolution limit of EDX mapping measurements and that the thickness of each phase cannot be completely the same between mapping and bright-field images. The peaks at 8.0 and 8.9 keV in (a) indicate the existence of a copper element, which agrees with the use of a copper grid.

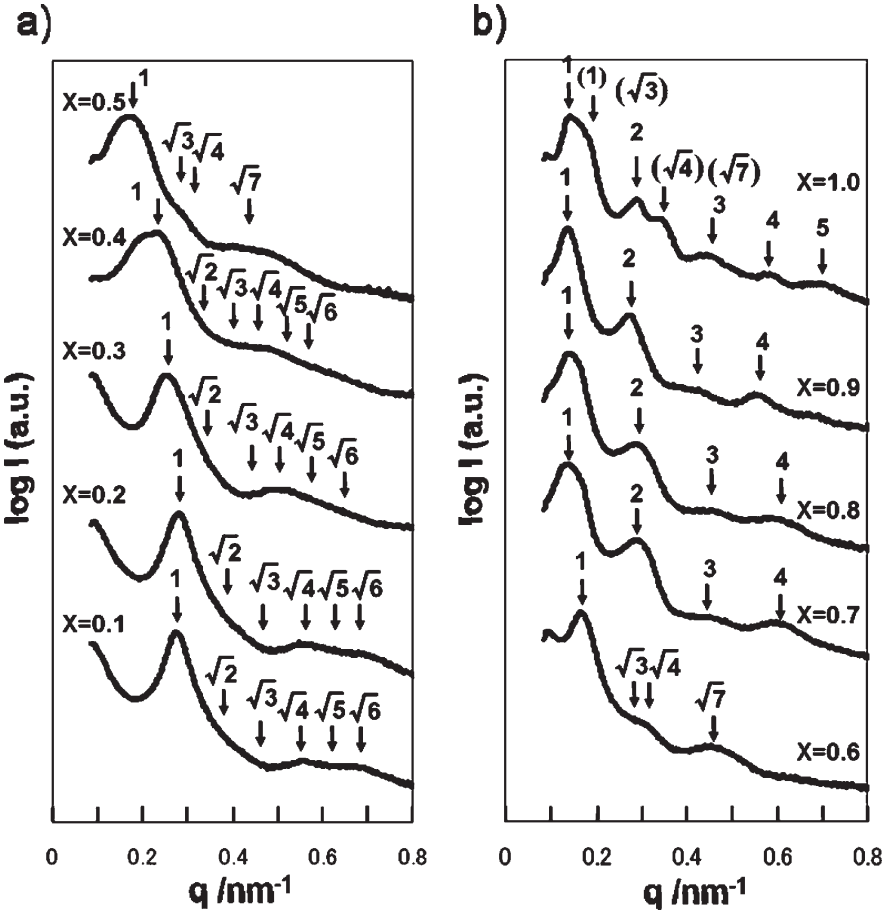


**Figure 6.** SAXS profiles of Fe(X): (a) Fe($X$) ($X$ = 0.1−0.5); (b) Fe($X$) ($X$ = 0.6−1.0).

higher $q$ regions than those of a neat block copolymer by addition of $FeCl_3$ at a lower amount such as $X$ = 0.1 and 0.2, and the peak positions tend to be located at lower $q$ regions if $X$ is larger than 0.3. This suggests that $D$ decreases by addition of a small amount of $FeCl_3$ and then turns to increase with a larger amount of $FeCl_3$. As for Fe(0.5) and Fe(0.6), there are characteristic peaks at the relative $q$ of 1, $3^{1/2}$, $4^{1/2}$, and $7^{1/2}$, suggesting cylindrical structures. These results are consistent with the TEM results. Note the profile of Fe(0.4) shows a quite broad peak with the $q$ position around 0.2 $nm^{-1}$, which might consist of two peaks with the first peak of a spherical structure (0.23 $nm^{-1}$) and that of a cylindrical structure (0.19 $nm^{-1}$), supporting that Fe(0.4) possesses the intermediate composition in a morphological phase diagram for the hybrid. There are simple and multiple integer order peaks on the profiles of Fe(0.7), F(0.8), and Fe(0.9), indicating lamellar structures, the results being consistent with TEM images.

On the other hand, the profile of Fe(1.0) has multiple peaks which cannot be assigned to a single nanophase-separated structure. This could be understood if Fe(1.0) forms two types of nanophase-separated structures: lamellae and cylinders, with the overflow of $FeCl_3$. Peaks at 0.14, 0.29. 0.44, and 0.59 $nm^{-1}$ could be assigned to the integer order peaks from lamellae, while a shoulder at 0.17 $nm^{-1}$ and the following peaks at 0.29, 0.35, and 0.45 $nm^{-1}$ could be regarded as peaks from a cylindrical structure: 1, $3^{1/2}$, $4^{1/2}$, and $7^{1/2}$ at relative $q$ values if the shoulder at 0.17 $nm^{-1}$ is regarded as the (100) reflection for a cylindrical structure. This assumption that 0.17 $nm^{-1}$ is the position of the first peak of a cylinder structure might be reasonable because the first peaks appear at around this $q$ region on the profiles of cylinder-forming hybrids such as Fe(0.5) and Fe(0.6). The result and analysis are quite consistent with the TEM results in Figure 4, i.e., macrophase separation between nanophase-separated regions of the hybrid. The reasons of such macrophase separation will be discussed in the Discussion section.

## Discussion

**$FeCl_3$ as a Filler with Noncovalent Bonding Interactions.** Even though the added $FeCl_3$ is an inorganic component with totally different chemical and physical properties from a block copolymer as an organic component, it can be homogeneously mixed with a P4VP phase up to 0.9 mol equiv of $FeCl_3$ to pyridine units in PS−P4VP. In fact, most of the Fe($X$) hybrids showed comparatively clear and single nanophase-separated structures. In addition, morphology transition from spherical structures to alternating lamellae by way of cylinders has occurred as the amount of $FeCl_3$ increases, accompanying the phenomenon of domain expansion. According to the simulation about the blend of a block copolymer and metal nanoparticles,[40] phase separation at the macroscopic scale due to the overflow of nanoparticles did not occur if the size of nanoparticles is smaller than the radius of gyration for the block. Our experimental results are consistent with this simulation if a metal salt used in this study is regarded as a very small particle.

As for the morphology transition, some systematic works were already known. They were reporting on morphology transition with domain expansion phenomenon by the addition of homopolymers.[74−76] Taking account of these systematic works, the added $FeCl_3$ could be regarded just as

a filler in P4VP phase as a small homopolymer in block copolymer/homopolymer blends, which could change the curvature of domain boundary between PS and P4VP phases, leading the morphology transition. This speculation is applicable to our results for Fe($X$) ($X > 0.2$). The domain size decreases from that of a neat PS−P4VP when the amount of $FeCl_3$ is smaller than 0.3 mol equiv to pyridine units in PS−P4VP, the results being reasonable if we refer to the similar works on block copolymer/metal chloride blends with intermolecular coordination.[63,64] This phenomenon might be explained by decrease in the average number of pyridine units coordinating to one $FeCl_3$, i.e., the degree of cross-linking induced by one $FeCl_3$. When the amount of $FeCl_3$ is less than 0.33, the degree of cross-linking induced by $FeCl_3$ is three, and the domain spacing tends to shrink due to the larger effect of cross-linking. However, as the amount of $FeCl_3$ becomes larger than 0.33, the degree of cross-linking should be less than three, which makes the effect of a filler larger, leading the increase in $D$-spacing. In any event, the addition of 0.9 mol equiv of $FeCl_3$ produces comparatively homogeneous nanophase-separated structures in each hybrid film if a solvent with coordination ability such as pyridine was used.

**Overflow of $FeCl_3$ from Nanophase-Separated Domains in the Sample with a Large Amount of $FeCl_3$.** Most Fe($X$) hybrid samples showed homogeneous morphology, i.e., single nanophase-separated structures. On the other hand, the overflow of $FeCl_3$ from the ordered nanostructure was evidently observed for Fe(1.0) by both TEM and SAXS.

To understand this phenomenon, it should be mentioned that $FeCl_3$ starts to coordinate with pyridine units in P4VP blocks at the final stage of solvent-casting as shown in Figure 1c, which helps the stable formation of hybrids between inorganic $FeCl_3$ and organic PS−P4VP. Note pyridine used as a solvent is useful as an inhibitor for rapid cross-linking of P4VP blocks at the initial stage of blending. Normally, each $FeCl_3$ can form a complex with three molar ligands via metal-to-ligand coordination. Therefore, $FeCl_3$ can hold three pyridine molecules as ligands at the initial stage of solvent-casting; however, $FeCl_3$ might replace a pyridine molecule as a ligand with a pyridine unit in P4VP one-by-one at the final stage of solvent-casting or at the stage of thermal annealing. This suggests that there could be a saturation limit for incorporation of $FeCl_3$ around the mole ratio of 1.0. In other words, stoichiometry is the dominant factor to control the morphology of the present hybrids.

## Summary

In conclusion, we have carried out a systematic study on preparation and morphology control of macroscopically homogeneous hybrid films composed of a block copolymer and a metal salt, where one block interacts with a metal salt by metal-to-ligand coordination. PS−P4VP was used as a block copolymer and iron(III) chloride ($FeCl_3$) was used as a metal salt in this study, and they were blended by changing the mole fraction of $FeCl_3$. To prevent the rapid cross-linking formation between P4VP and $FeCl_3$ during solvent casting, pyridine as a polar solvent with the coordination ability was used at the solvent-casting stage, which serves as an effective agent to prepare macroscopically homogeneous films with a large amount of $FeCl_3$. Morphology at the nanoscopic scale of all samples was observed by both TEM and SAXS. It was revealed that $FeCl_3$ can be homogeneously mixed with P4VP, which results in forming simple ordered nanostructures up to 0.9 mol equiv to pyridine units in PS−P4VP, where $FeCl_3$ works as a filler in a P4VP phase just as small homopolymers. The domain expansion and morphology transition were observed as the amount of added $FeCl_3$ increases. However, isolation of a $FeCl_3$ phase was also recognized in the hybrid sample with the amount of 1.0 mol equiv of $FeCl_3$, which might be owing to the saturation of incorporated $FeCl_3$. All of these results will provide the useful guide to design the hybrids consisting of block copolymers and metal salts.

**Acknowledgment.** A.N. thanks Grant-in-Aid for Young Scientists (B) (No. 21750217) from Ministry of Education, Culture, Sports and Science, and Technology of Japan. Use of the synchrotron X-ray source was supported by Photon Factory, KEK in Tsukuba, Japan (No. 2008G187 and 2010G059 for A.N.). This work was partially supported by the Global COE Program in Chemistry entitled "Elucidation and Design of Materials and Molecular Functions" and Grant-in-Aid for Scientific Research on Priority Area "Soft Matter Physics" (No. 18068008) from the Ministry of Education, Culture, Sports and Science, and Technology of Japan.

**Supporting Information Available:** Details of synthesis and characterization of polymers. This material is available free of charge via the Internet at http://pubs.acs.org.

## References and Notes

(1) Usuki, A.; Kojima, Y.; Kawasumi, M.; Okada, A.; Fukushima, Y.; Kurauchi, T.; Kamigaito, O. *J. Mater. Res.* **1993**, *8*, 1179–1184.
(2) Vaia, R. A.; Ishii, H.; Giannelis, E. P. *Chem. Mater.* **1993**, *5*, 1694–1696.
(3) Ray, S. S.; Okamoto, M. *Prog. Polym. Sci.* **2003**, *28*, 1539–1641.
(4) Huynh, W. U.; Dittmer, J. J.; Alivisatos, A. P. *Science* **2002**, *295*, 2425–2427.
(5) Coronado, E.; Galan-Mascaros, J. R.; Gomez-Garcia, C. J.; Laukhin, V. *Nature* **2000**, *408*, 447–449.
(6) Mirkin, C. A.; Letsinger, R. L.; Mucic, R. C.; Storhoff, J. J. *Nature* **1996**, *382*, 607–609.
(7) Boal, A. K.; Ilhan, F.; DeRouchey, J. E.; Thurn-Albrecht, T.; Russell, T. P.; Rotello, V. M. *Nature* **2000**, *404*, 746–748.
(8) Kitagawa, S.; Kitaura, R.; Noro, S. *Angew. Chem., Int. Ed.* **2004**, *43*, 2334–2375.
(9) Eddaoudi, M.; Moler, D. B.; Li, H. L.; Chen, B. L.; Reineke, T. M.; O'Keeffe, M.; Yaghi, O. M. *Acc. Chem. Res.* **2001**, *34*, 319–330.
(10) Matsuo, M.; Ueno, T.; Horino, H.; Chujyo, S.; Asai, H. *Polymer* **1968**, *9*, 425.
(11) Leibler, L. *Macromolecules* **1980**, *13*, 1602–1617.
(12) Ohta, T.; Kawasaki, K. *Macromolecules* **1986**, *19*, 2621–2632.
(13) Bates, F. S.; Fredrickson, G. H. *Annu. Rev. Phys. Chem.* **1990**, *41*, 525–557.
(14) Matsen, M. W.; Bates, F. S. *Macromolecules* **1996**, *29*, 1091–1098.
(15) Lodge, T. P. *Macromol. Chem. Phys.* **2003**, *204*, 265–273.
(16) Matsushita, Y. *Macromolecules* **2007**, *40*, 771–776.
(17) Segalman, R. A.; McCulloch, B.; Kirmayer, S.; Urban, J. J. *Macromolecules* **2009**, *42*, 9205–9216.
(18) Simon, P. F. W.; Ulrich, R.; Spiess, H. W.; Wiesner, U. *Chem. Mater.* **2001**, *13*, 3464–3486.
(19) Bockstaller, M. R.; Mickiewicz, R. A.; Thomas, E. L. *Adv. Mater.* **2005**, *17*, 1331–1349.
(20) Balazs, A. C.; Emrick, T.; Russell, T. P. *Science* **2006**, *314*, 1107–1110.
(21) Shenhar, R.; Norsten, T. B.; Rotello, V. M. *Adv. Mater.* **2005**, *17*, 657–669.
(22) Glogowski, E.; Tangirala, R.; Russell, T. P.; Emrick, T. *J. Polym. Sci., Polym. Chem.* **2006**, *44*, 5076–5086.
(23) Fahmi, A.; Pietsch, T.; Mendoza, C.; Cheval, N. *Mater. Today* **2009**, *12*, 44–50.
(24) Ober, C. K.; Cheng, S. Z. D.; Hammond, P. T.; Muthukumar, M.; Reichmanis, E.; Wooley, K. L.; Lodge, T. P. *Macromolecules* **2009**, *42*, 465–471.
(25) Deng, L.; Furuta, P. T.; Garon, S.; Li, J.; Kavulak, D.; Thompson, M. E.; Frechet, J. M. J. *Chem. Mater.* **2006**, *18*, 386–395.
(26) Marin, V.; Holder, E.; Hoogenboom, R.; Schubert, U. S. *Chem. Soc. Rev.* **2007**, *36*, 618–635.
(27) Weck, M. *Polym. Int.* **2007**, *56*, 453–460.
(28) Aamer, K. A.; De Jeu, W. H.; Tew, G. N. *Macromolecules* **2008**, *41*, 2022–2029.
(29) Shunmugam, R.; Tew, G. N. *Macromol. Rapid Commun.* **2008**, *29*, 1355–1362.
(30) Fox, J. D.; Rowan, S. J. *Macromolecules* **2009**, *42*, 6823–6835.

(31) Ni, Y. Z.; Rulkens, R.; Manners, I. *J. Am. Chem. Soc.* **1996**, *118*, 4102–4114.
(32) Cheng, J. Y.; Ross, C. A.; Chan, V. Z. H.; Thomas, E. L.; Lammertink, R. G. H.; Vancso, G. J. *Adv. Mater.* **2001**, *13*, 1174.
(33) Temple, K.; Kulbaba, K.; Power-Billard, K. N.; Manners, I.; Leach, K. A.; Xu, T.; Russell, T. P.; Hawker, C. J. *Adv. Mater.* **2003**, *15*, 297–300.
(34) Rider, D. A.; Cavicchi, K. A.; Power-Billard, K. N.; Russell, T. P.; Manners, I. *Macromolecules* **2005**, *38*, 6931–6938.
(35) Eloi, J. C.; Rider, D. A.; Wang, J. Y.; Russell, T. P.; Manners, I. *Macromolecules* **2008**, *41*, 9474–9479.
(36) Bockstaller, M. R.; Lapetnikov, Y.; Margel, S.; Thomas, E. L. *J. Am. Chem. Soc.* **2003**, *125*, 5276–5277.
(37) Costanzo, P. J.; Beyer, F. L. *Macromolecules* **2007**, *40*, 3996–4001.
(38) Li, C. P.; Wu, C. H.; Wei, K. H.; Sheu, J. T.; Huang, J. Y.; Jeng, U. S.; Liang, K. S. *Adv. Funct. Mater.* **2007**, *17*, 2283–2290.
(39) Zhao, Y.; Thorkelsson, K.; Mastroianni, A. J.; Schilling, T.; Luther, J. M.; Rancatore, B. J.; Matsunaga, K.; Jinnai, H.; Wu, Y.; Poulsen, D.; Frechet, J. M. J.; Alivisatos, A. P.; Xu, T. *Nature Mater.* **2009**, *8*, 979–985.
(40) Huh, J.; Ginzburg, V. V.; Balazs, A. C. *Macromolecules* **2000**, *33*, 8085–8096.
(41) Thompson, R. B.; Ginzburg, V. V.; Matsen, M. W.; Balazs, A. C. *Science* **2001**, *292*, 2469–2472.
(42) Lee, J. Y.; Thompson, R. B.; Jasnow, D.; Balazs, A. C. *Phys. Rev. Lett.* **2002**, 89.
(43) Yeh, S. W.; Wei, K. H.; Sun, Y. S.; Jeng, U. S.; Liang, K. S. *Macromolecules* **2005**, *38*, 6559–6565.
(44) Spontak, R. J.; Shankar, R.; Bowman, M. K.; Krishnan, A. S.; Hamersky, M. W.; Samseth, J.; Bockstaller, M. R.; Rasmussen, K. O. *Nano Lett.* **2006**, *6*, 2115–2120.
(45) Matsen, M. W.; Thompson, R. B. *Macromolecules* **2008**, *41*, 1853–1860.
(46) Warren, S. C.; Messina, L. C.; Slaughter, L. S.; Kamperman, M.; Zhou, Q.; Gruner, S. M.; DiSalvo, F. J.; Wiesner, U. *Science* **2008**, *320*, 1748–1752.
(47) Yabu, H.; Koike, K.; Motoyoshi, K.; Higuchi, T.; Shimomura, M. *Chem. Lett.* **2009**, *38*, 964–965.
(48) Zorn, M.; Bae, W. K.; Kwak, J.; Lee, H.; Lee, C.; Zentel, R.; Char, K. *ACS Nano* **2009**, *3*, 1063–1068.
(49) Lin, Y.; Boker, A.; He, J. B.; Sill, K.; Xiang, H. Q.; Abetz, C.; Li, X. F.; Wang, J.; Emrick, T.; Long, S.; Wang, Q.; Balazs, A.; Russell, T. P. *Nature* **2005**, *434*, 55–59.
(50) Li, Q. F.; He, J. B.; Glogowski, E.; Li, X. F.; Wang, J.; Emrick, T.; Russell, T. P. *Adv. Mater.* **2008**, *20*, 1462.
(51) Chiu, J. J.; Kim, B. J.; Kramer, E. J.; Pine, D. J. *J. Am. Chem. Soc.* **2005**, *127*, 5036–5037.
(52) Kim, B. J.; Chiu, J. J.; Yi, G. R.; Pine, D. J.; Kramer, E. J. *Adv. Mater.* **2005**, *17*, 2618.
(53) Chiu, J. J.; Kim, B. J.; Yi, G. R.; Bang, J.; Kramer, E. J.; Pine, D. J. *Macromolecules* **2007**, *40*, 3361–3365.
(54) Kim, B. J.; Fredrickson, G. H.; Kramer, E. J. *Macromolecules* **2008**, *41*, 436–447.
(55) Chan, Y. N. C.; Schrock, R. R.; Cohen, R. E. *J. Am. Chem. Soc.* **1992**, *114*, 7295–7296.
(56) Tsutsumi, K.; Funaki, Y.; Hirokawa, Y.; Hashimoto, T. *Langmuir* **1999**, *15*, 5200–5203.
(57) Ho, R. M.; Lin, T.; Jhong, M. R.; Chung, T. M.; Ko, B. T.; Chen, Y. C. *Macromolecules* **2005**, *38*, 8607–8610.
(58) Adachi, M.; Okumura, A.; Sivaniah, E.; Hashimoto, T. *Macromolecules* **2006**, *39*, 7352–7357.
(59) Lin, T.; Ho, R. M.; Ho, J. C. *Macromolecules* **2009**, *42*, 742–751.
(60) Mendoza, C.; Pietsch, T.; Gutmann, J. S.; Jehnichen, D.; Gindy, N.; Fahmi, A. *Macromolecules* **2009**, *42*, 1203–1211.
(61) Mendoza, C.; Gindy, N.; Gutmann, J. S.; Fromsdorf, A.; Forster, S.; Fahmi, A. *Langmuir* **2009**, *25*, 9571–9578.
(62) Lin, T.; Li, C. L.; Ho, R. M.; Ho, J. C. *Macromolecules* **2010**, *43*, 3383−3391.
(63) Lee, D. H.; Kim, H. Y.; Kim, J. K.; Huh, J.; Ryu, D. Y. *Macromolecules* **2006**, *39*, 2027–2030.
(64) Lee, D. H.; Han, S. H.; Joo, W.; Kim, J. K.; Huh, J. *Macromolecules* **2008**, *41*, 2577–2583.
(65) Convertine, A. J.; Sumerlin, B. S.; Thomas, D. B.; Lowe, A. B.; McCormick, C. L. *Macromolecules* **2003**, *36*, 4679–4681.
(66) Moad, G.; Rizzardo, E.; Thang, S. H. *Aust. J. Chem.* **2005**, *58*, 379–410.
(67) Lowe, A. B.; McCormick, C. L. *Prog. Polym. Sci.* **2007**, *32*, 283–351.
(68) Moad, G.; Rizzardo, E.; Thang, S. H. *Aust. J. Chem.* **2009**, *62*, 1402–1472.
(69) Lai, J. T.; Filla, D.; Shea, R. *Macromolecules* **2002**, *35*, 6754–6756.
(70) Noro, A.; Matsushita, Y.; Lodge, T. P. *Macromolecules* **2008**, *41*, 5839–5844.
(71) Noro, A.; Yamagishi, H.; Matsushita, Y. *Macromolecules* **2009**, *42*, 6335–6338.
(72) Noro, A.; Nagata, Y.; Tsukamoto, M.; Hayakawa, Y.; Takano, A.; Matsushita, Y. *Biomacromolecules* **2005**, *6*, 2328–2333.
(73) Hahn, H.; Chakraborty, A. K.; Das, J.; Pople, J. A.; Balsara, N. P. *Macromolecules* **2005**, *38*, 1277–1285.
(74) Tanaka, H.; Hasegawa, H.; Hashimoto, T. *Macromolecules* **1991**, *24*, 240–251.
(75) Matsen, M. W. *Macromolecules* **1995**, *28*, 5765–5773.
(76) Torikai, N.; Takabayashi, N.; Noda, I.; Koizumi, S.; Morii, Y.; Matsushita, Y. *Macromolecules* **1997**, *30*, 5698–5703.